Fall 2019

Methane dry reforming reaction on Cr, V, In, and Ga Supported SAPO-34 zeolite

Ehigiator Festus Ojo

Department:

METHANE DRY REFORMING REACTION ON Cr, V, In, AND Ga SUPPORTED SAPO-34 ZEOLITE

by

EHIGIATOR FESTUS OJO

A THESIS

Presented to the Faculty of the Graduate School of the

MISSOURI UNIVERSITY OF SCIENCE AND TECHNOLOGY

In Partial Fulfillment of the Requirements for the Degree

MASTER OF SCIENCE IN CHEMICAL ENGINEERING

2019

Approved by:

Ali Rownaghi, Advisor
Douglas Ludlow
Fateme Razaei

ABSTRACT

The CO_2 reforming of methane is a significant research area in mitigating and transforming two greenhouse gases for the production of syngas. The reaction has been investigated for four different promoted catalysts to determine their reactant's conversion, product's selectivity, and their respective syngas ratios.

The catalytic test was investigated under atmospheric conditions at 600ºC for 6.5h with a WHSV of 4800 ml g^{-1} h^{-1}. The conversion and selectivity of catalysts 9Al 1V-inc SAPO-34, 9Al 1Cr-inc SAPO-34, 9Al 1Ga-inc SAPO-34, and 9Al 1In-inc SAPO-34 were analyzed. The CH_4 conversion for the different catalysts are, 9Al 1Cr-inc SAPO-34 (33%), 9Al 1Y-inc SAPO-34 (27%), 9Al 1Ga-inc SAPO-34 (31%), and 9Al 1In-inc SAPO-34 (32%). The Cr promoted catalyst gave the highest CH_4 conversion and the highest syngas ratio of 0.7, while the In promoted catalyst gave the highest CO_2 conversion of 34%. The highest CO and H_2 selectivity (34% and 7%) was from 9Al 1V-inc SAPO-34 catalyst. The different conversion, selectivity, and syngas ratio obtained for these catalysts is a result of the different bimetallic metal (alloy) used on the weakly acidic zeolite support.

The heat and mass transfer limitations on the catalysts were analyzed using the Weiz-Prater criteria for internal diffusion, the Mears criterion for external diffusion, and combined interphase and intraparticle heat and mass transfer. Based on the evaluated report, there was no heat and mass transfer limitations on these catalysts.

ACKNOWLEDGMENTS

I want to specially thank the faculty and staff of the Department of Chemical and Biological Engineering for the resources put in place to make this research work a success.

I want to thank the best advisor in the Department of Chemical and Biological Engineering, Dr. Ali Rownaghi, for accepting me as a research student and believing in me to complete this work. I say a big thank you to Dr. Douglas Ludlow and Dr. Fateme Razaei for their unique support. Also, I want to say a big thank you to Fatima Magzoub, Abbas Jawad, and Busuyi Adebayo, Ph.D. candidates, for their support during this research. I want to sincerely thank my family, especially my mother, for her huge support during the course of this program. Moreover, I want to say a special thank you to all the Catalysis Research Group for their support during this research work. A special thanks to Kyle Newport and Joseph Saitta, undergraduate students, who helped and demonstrated great skills in supporting this research. Above all, thanks to God Almighty for granting me a special ability to complete this research work.

TABLE OF CONTENTS

Page

LIST OF ILLUSTRATIONS

LIST OF TABLES

NOMENCLATURE

Symbol	Description
ΔH	Heat of Reaction, KJ / mol
ΔG	Change in Gibbs Free Energy, KJ / mol
C_{wp}	Weiz- Prater Criterion
$-r_{A(obs)}$	Observed Reaction Rate, mol / kg cat. s
R	Catalyst Particle Radius, m
ρ_c	Solid Catalyst Density, kg / m^3
ρ_b	Bulk Density of Catalyst Bed, kg /m^3
D_e	Effective Gas-Phases Diffusivity, m^2 / s
D_{AB}	Gas-Phases Diffusivity, m^2 / s
C_{As}	Gas Concentration of A at the Catalyst Surface, Kmol – A / m^3
C_{Ab}	Bulk Gas Concentration of A, Kmol – A / m^3
K_c	Mass Transfer Coefficient, m / s
E_a	Activation Energy, KJ / mol
R_g	Gas Constant, KJ / mol. K
h_f	Heat Transfer coefficient between gas and pellet, W/ m^2K
γ	Arrhenius number
β_b	Heat generation function
λ	Catalyst thermal conductivity, W/ m.K
χ	Damköhler number for interphase heat transport
ω	Damköhler number for interphase mass transport

1. INTRODUCTION

The world today is craving an alternative form of energy because of the over-dependence on fossil fuels; it is causing serious environmental issues like global warming. In recent years, researchers have developed new ways to replace these fossil fuels as the world energy source, resulting in the use of natural gas energy sources. CH_4 is the most abundant source of natural gas about 98% of natural gas is made up of CH_4. CH_4 and CO_2 are greenhouse gases, while CO_2 emission has the highest impact on global warming contributing about 9-26% of the greenhouse gases, and methane contributes to about 4-9%. The percentage of CO_2 is expected to rise to a record level from 541 to 970 ppm by the year 2100 according to the intergovernmental panel on climate change [1]. The development of a suitable catalyst that will kinetically limit the formation of carbon by the subsequent oxidation of the carbon species formed on the surface of the metal is critical to boost the DRM reaction rate. Conversion of these greenhouse gases to useful raw chemicals like syngas is vital to reducing global warming and producing raw materials for the Fischer – Tropsch synthesis [2]. Also, the dry reforming of methane to produce syngas [Eq. (1)] that is desirable for the Fischer – Tropsch process is gaining attention all around the world because of its environmental benefit of mitigating greenhouse gases (CO_2 and CH_4). An alternative route to produce syngas with a ratio of less than 1, which is influenced by the simultaneous reverse water gas shift reaction [3], is very valuable for the F-T process. Although, the development of a suitable catalyst for an industrial scale remains a challenge due to the high-temperature requirement of 700-900ºC and synthesizing a catalyst that is less susceptible to deactivation due to carbon formation. So, developing and

testing a suitable catalyst for DRM to meet the scale-up requirements is key to this research [4][5]. The steam reforming of methane (SRM) is adopted industrially for the production of syngas but requires a high reaction temperature of 800-900^{o}C. This also requires an enormous amount of steam and subsequent pretreatment of the high H_2/CO ratio for the Fischer- Tropsch process [1] [5] [4]. The partial oxidation of methane (POM), which is another process utilized for the production of syngas, has the challenge of the high cost of procuring oxygen. The production of hotspots during the reaction at high temperature (exothermicity) is another problem faced with POM [5]. The synthesis, characterization, and testing of these catalysts to meet the requirement for an industrial scale syngas yield is of high importance in this research. The effective utilization of these greenhouse gases could stem from the fact energy used for this process should be from a renewable source like solar energy or nuclear energy. The major fossil energy component, like natural gas, is used in gas-fired power plants. The dry reforming of methane, a highly endothermic reaction, could give rise to high purity syngas with a lower H_2/CO ratio, (which is nearly 1), required for the Fischer- Tropsch process as the feedstock for the production of transportation fuel and other valuable products, like light hydrocarbons. This could give rise to the formation of transportation fuel like DME. During dry reforming of methane, coke formation from atomic carbon could be attributed to the activation of methane molecule [Eq. (2)], or during the Boudouard reaction [Eq. (3)] [6] [7]. The greenhouse gases, methane, and CO_2 are gas mixtures extracted from natural gas as final products and are converted to environmentally useful products like syngas at low cost [8]. The availability of syngas as a feed-stock in the production of extremely clean liquid fuels like Methanol, DME, gasoil, and gasoline with no traceable amount of Sulphur content and

reduced quantity of aromatics via the Fischer-Tropsch process highlights one of the benefits of using syngas as a raw material for this process. Natural gas is not the only source of CH_4 and CO_2. The constituents found in high concentration of Landfill gas, also known as biogas, produced from the decomposition of organic matter and are composed of 45-55% CH_4, 30-40% CO_2, 0-5% O_2, and the remaining N_2. These deposits are composed of about 37-57 million tons of CH_4 which consist of 13-20% of total United States methane (CH_4) production. There are different technologies employed in the reforming of CH_4 to syngas (H_2 and CO), and these include, steam reforming (SR), dry reforming of methane (DRM), partial oxidation (PO), and auto-thermal reforming (AR). The distinction between these technologies lies in the type of oxidant used, H_2/CO product ratio, and the kinetics and energetics of the reaction process. Among these technologies, dry reforming of methane, which is highly endothermic, is susceptible to deactivation by carbon formation, sintering of the metal particle, and support at elevated temperatures. The DRM process has the smallest operating cost of about 20% when compared to other technologies according to Ross et al. [1] [9]. The zeolite support, siliconaluminophosphate (SAPO-34), is a micro-porous zeolite, which has Brönsted and Lewis acid sites; it is resistant to hydrothermal treatment stem from the silicon acid site. The zeolite with chabazite framework was used because of its unique properties such as high surface area, mild acidity, large cages, small windows, high thermal stability, and high CO_2 affinity [10]. The support SAPO-34 is synthesized by inserting Si in the ALPO framework [11] [12]. The SAPO-34 is chosen as a support because of its resistance to coke formation and its stability, which is a result of its low acid site density and hierarchical structure [11]. The hierarchical structure plays an important role in reducing diffusion within the zeolite by mitigating the steric effect. It

should be noted that the unique catalytic properties of the SAPO -34 is based on the how the Silicon is dispersed on the CHA framework [10] [13] [14]. The zeolite catalyst can disperse the alloy used; this, in turn, makes the catalyst less prone to coke deactivation and provide the unique stability observed for DRM reaction [15]. The activation of methane could be challenging to scientists and researchers because it is thermodynamically stable [16]. In DRM reactions, one of the most important side reaction is the reverse water gas shift reaction (RWGS) reaction, which influences the production of a syngas ratio of less than 1, and it is represented by [Eq. (4)][17]. The purpose of this research is to test the catalytic activity of the different alloys incorporated into the chazabite zeolite framework catalysts at 600ºC and 1atm since it has been reported that high equilibrium conversion for CH_4 and CO_2 can be obtained at 800-1000 for the DRM reaction [7]. Another aspect of this research was to determine the mass and heat transfer limitations on the four catalysts using the highest reaction rates. This criterion becomes necessary for scale-up purposes [18].

$$\begin{aligned} &CH_4 + CO_2 \rightleftharpoons 2CO + 2H_2 \\ &\Delta H_{298K} = +247 KJ/mol \\ &\Delta G_{298K} = +170 KJ/mol \end{aligned} \tag{1}$$

$$\begin{aligned} &CH_4 \rightleftharpoons C + 2H_2 \\ &\Delta H^{o}_{298K} = 75 KJ/mol \\ &\Delta G^{o}_{298K} = 2190 - 26.45T \end{aligned} \tag{2}$$

$$\begin{aligned} &2CO \rightleftharpoons CO_2 + C \\ &\Delta H^{o}_{298K} = -171 KJ/mol \\ &\Delta G^{o}_{298K} = -39810 + 40.87T \end{aligned} \tag{3}$$

$$\begin{aligned} &CO_2 + H_2 \rightleftharpoons CO + H_2O \\ &\Delta H^{o} = -41 KJ/mol \end{aligned} \tag{4}$$

2. METHODOLOGY

The incorporation of different metal promoters such as Vanadium (V), Indium (In), Gallium (Ga), and Chromium (Cr) into chazabite framework of the zeolite support demonstrated useful catalytic activity for the dry reforming of methane. The chemical process used for the incorporation of these promoters was the hydrothermal synthesis method. Because the isomorphous substitution method was used, the catalyst is known to have a well mono–dispersed active phase of the metal promoter on the zeolite support. This method was used because of its ability to improve catalytic performance and initiate active sites making the catalyst more selective.

2.1. CATALYST SYNTHESIS

The way catalysts are prepared has a significant effect on its performance and activity. The different catalysts used in this research were prepared using the hydrothermal crystallization method. The precursors used in synthesizing these four catalysts were obtained from Sigma-Aldrich, while the tetraethylammonium hydroxide template was purchased from SACHEM chemical company. The synthesis of SAPO-34 support mixture was achieved with a molar ratio reported in literature. The addition of 40ml of H_2O with roughly 26.71 g of TEAOH in 35 wt% water SACHEM grade for 45min. produced an aqueous solution of tetraethyl aluminum hydroxide in four places respectively. The dropwise addition of 7.2g of orthophosphoric acid (85 wt% Sigma-Aldrich) to each of the four solutions was stirred for 15mins. Another dropwise addition of 1.72 g of tetraethyl

orthosilicate (98% Sigma-Aldrich) to the four solution was stirred continuously at 725 rpm for 2hs.

The Al/metal ratio used is 9:1. These catalysts (9Al 1Ga-SAPO-34, 9Al 1In-SAPO-349Al 1V-SAPO-34, 9Al 1Cr-SAPO-34) were finally synthesized when 2.12 g of Gallium Nitrate Hydrate, 1.8 g of Indium Nitrate Hydrate (99.9% Sigma-Aldrich), 1.11 g of Vanadium (111) Chloride, and 2.82g of Chromium (111) Nitrate Nonahydrate were put in each of the four solutions in a Teflon-lined autoclave. The various added were dissolved by stirring for 15min., then 12.97 g of $C_9H_{21}O_3Al$ was added dropwise to the four solutions and was stirred continuously for 100min. The added $C_9H_{21}O_3Al$ is equivalent to the aluminum/metal ratio of 9:1. The pH of the solution was altered to neutral by adding 2.19 g of HCl, and the solution was stirred for 70mins. The molar ratio of the solution is in this order 1.0 Al_2O_3, 1.0 P_2O_5, 0.26 SiO_2, 2.0 TEAOH, 70 H_2O, and 0.7 HCl. The hydrothermal synthesis was then performed when the solution/sample was moved to Teflon- lined autoclaves, and then put in a VWR gravity convection oven @ 200 °C for 24hs.

The catalysts were washed a number times by sequential centrifuging at 400 rpm for 15 mins., and then they were dried at 110 °C for 24 hours. The calcination of the catalyst was performed in an F6000 oven at 600 °C for 6 hs.

2.2. CATALYST CHARACTERIZATION

The characterization of each catalyst was performed by different techniques to have a better understanding of the activity of the catalysts during the dry reforming of methane. X-ray diffraction was used to determine the crystallinity and phase purity of the catalyst while the Scanning Electron Microscopy (SEM) was used to investigate the morphology

and topology of the synthesized catalysts. The Textural properties of the catalyst was determined by using a technique called nitrogen physisorption. The acidic properties of the catalyst were analyzed using Temperature Programmed Desorption of Ammonia (NH_3-TPD). It also helps in defining the unique properties of the catalysts employed in this process. The techniques employed for the characterization of these catalysts are discussed below.

2.2.1. X-ray Diffraction. This technique, powder X-ray diffraction, is important in determining the crystallinity and phase purity of the catalysts. The XPERT-PRO diffractometer, accompanied by Cu $k\alpha$ radiation (λ = 1.540598) at 45 kV and 40 mA, scanned the catalysts continuously for 2θ the range of 5° 5 to 50° 50 degrees. The Sherrer Equation [Eq. (5)] was used to determine the crystallite sizes obtained from the XRD spectra.

$$d = \frac{0.089\lambda}{B(2\theta)\cos\theta} \tag{5}$$

where λ = 1.54056 Å, $B(2\theta)$ is the peak at full width half maximum (FWHM) and θ is the angle in radians. The diffraction pattern is shown below in Figure 4.1.

2.2.2. Scanning Electron Microscopy (SEM). The Scanning Electron Microscopy (SEM) technique was used to determine the topology and the morphology of the different catalysts being investigated. Surface charge effects were mitigated by coating the samples (catalysts) with gold before the images were taken with an electron microscope operating at 20kV.

2.2.3. Nitrogen Physisorption Measurements. This technique is useful for determining the textural properties of the catalyst samples. This process was carried out on a micromeritics 3FLEX Surface Characterization Analyzer at -196°C. the degassing of the catalyst samples were necessary to remove moisture content before analysis, and this was performed under vacuum at 250°C for 12hs. The data from the adsorption isotherm was used to calculate the specific surface area of the different catalysts using the Brunauer-Emmett-Teller (BET) method with a relative pressure (P/P_o) range of 0.05 to 0.1. Moreover, the Barret-Joyner-Halenda (BJH) method for pore size distribution was also used to determine the pore size, pore diameter, and total pore size from the adsorption arm of the isotherm based on the modified form of the Kevin Equation as shown in Table 4.3.

2.2.4. Temperature Programmed Desorption of Ammonia (NH_3 – TPD). This technique was used to analyze the acid properties of the four catalysts investigated. Ammonia was used in this experiment because its small size allows the molecule to penetrate the pores of the zeolite support and act reciprocally with both BrØnsted and Lewis acid sites [19]. The experiment was carried out on micromeritics 3FLEX 543 analyzer employing 10% H_2 in an Air mixture at a flow rate of 50cm^3/min. The sample (~ 100mg) was placed in a U – type quartz reactor, which was then preheated by passing dry helium (99.99%) at 500°C for 1h. The process was immediately cooled to 100°C in the presence of the flowing helium. This process was carried out before the adsorption of ammonia. At 100°C, the catalyst samples were saturated with NH_3 for 2 hours and He was passed at the same temperature for half an hour to separate physically adsorbed ammonia.

Subsequently, with a temperature of 700°C, a heating rate of 10°C/min, and uninterrupted flow of He, the quantity of NH_3 desorbed was analyzed by Quadrupole Mass Spectrometer (BEL Japan). The data for various BrØnsted and Lewis sites are given in Figure 4.6.

3. EXPERIMENT

The catalytic test was carried out using an on-line (SRI 8610C) gas chromatograph (GC) equipped with FID and TCD to analyze the products (syngas). The GC was connected to a stainless steel down-flow fixed bed reactor with an inside diameter of 10mm, a length of 300mm, and a type-K thermocouple that was inserted into the reactor to monitor the temperature of the reactor for 6.5h. The catalysts were prepared using the hydrothermal crystallization method. Additionally, 0.5g of the catalyst was mixed with quartz sand (particle size 0.5μm) using a ratio of 1:6. The catalyst was loaded into the reactor; quartz wool was used in the reactor both at the top and at the bottom of the reactor to stabilize the catalyst inside the reactor. Different catalysts were tested isothermally at 600ºC for 6.5h hours on stream using a constant flowrate of 53.23ml/min. The gas mixture, 50.27% CH4 purity and 49.73% CO2 purity was fed to the reactor through a line connected to a cylinder at 52.23ml/min with a pressure of 1bar. The effluent stream was analyzed with thermal conductivity detector (TCD) and FID chromatograph connected to the online gas chromatograph, which was used to analyze hydrocarbon products (C_1-C_6). The TCD was used to examine the CO_2, H_2, and CO products. The primary product of interest in this research is the syngas (H2 and CO). The conversion of the reactants (CH_4 and CO_2) was calculated using [Eq. (6)] and [Eq. (7)]. Before DRM reaction, the catalyst was purged with N_2 (40mL.min^{-1}) for 1h. at 600ºC, and air was passed through catalysts for 10 min. to release the water content. The schematic representation of the experimental process is shown in Figure 3.1. The selectivity of H_2 and CO was calculated with [Eq. (8)] and [Eq. (9)].

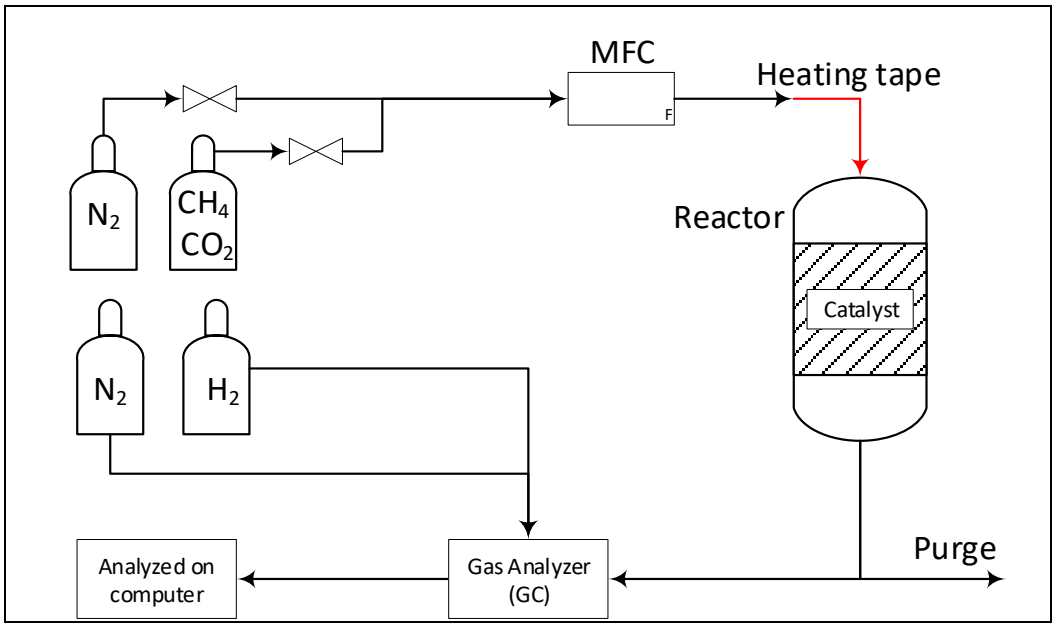

Figure 3.1. Schematic Representation of the DRM Process

$$X_{CH_4}(\%) = 100 * \frac{[CH_4]_{In} - [CH_4]_{Out}}{[CH_4]_{In}} \quad (6)$$

$$X_{CO_2}(\%) = 100 * \frac{[CO_2]_{In} - [CO_2]_{Out}}{[CO_2]_{In}} \quad (7)$$

$$S_{H_2}(\%) = 100 * \frac{[H_2]_{Out}}{2 * [CH_4]_{In} - [CH_4]_{Out}} \quad (8)$$

$$S_{CO}(\%) = 100 * \frac{[CO]_{Out}}{[CH_4]_{In} - [CH_4]_{Out} + [CO_2]_{In} - [CO_2]_{Out}} \quad (9)$$

where, $[CH_4]_{In}$ = blank area, $[CH_4]_{out}$ = exit area for methane gas, and $[CO_2]_{in}$, $[CO2]_{out}$,

and $[CO]_{out}$ are blank area, exit area of carbon dioxide gas, and exit carbon monoxide gas respectively.

The mass and heat transfer calculations were carried out using the Weisz-Prater criterion [Eq. (10)] to determine the internal diffusion limitation. The Mears criterion [Eq. (11)] was used to determine the combined interface and intraparticle heat and mass transfer limitations. The effect of external diffusion was investigated using the Mears criterion for external diffusion [Eq. (12)]

$$C_{WP} = \frac{-r'_{A(obs)}\rho_c R^2}{D_e C_{As}} < 1 \tag{10}$$

$$\frac{-r'_A R^2}{C_{Ab} D_e} < \frac{1 + 0.33\gamma\chi}{|n - \gamma_b \beta_b|(1 + 0.33\mathrm{n}\omega)} \tag{11}$$

$$\frac{-r'_A \rho_b R n}{K_c C_{Ab}} < 0.15 \tag{12}$$

The effect of temperature variation between the bulk fluid and the surface of the catalyst was also evaluated using [Eq. (13)]. These limitations were developed based on the highest reaction rates observed for the four catalysts being investigated.

$$\left| \frac{-\Delta H(-r'_A)\rho_b R E}{h_f T_b^2 R_g} \right| < 0.15 \tag{13}$$

4. RESULTS AND DISCUSSIONS

The result of the characterization of the catalysts and the catalytic activities are discussed in details in this section to understand the unique behavior of the different catalysts.

4.1. X-RAY DIFFRACTION ANALYSIS OF THE CATALYSTS

The four catalysts investigated using this technique gave different x-ray diffraction pattern as shown in Figure 4.1. A characteristic diffraction peak was observed for the SAPO-34 CHA framework in agreement with literature [20] [21]. A different peak was also observed at 2theta = 7.6° which could suggest the presence of crystallization of unreacted species. The other peaks observed at 2theta = 9.6, 13, 16, 20.6, 22.5, 26 and 30.7° is in agreement with the diffraction at (100), (101), (111), (200), (201), (211), and (310) crystal lattice plane. This is also in agreement with a typical chazabite structure as reported in literature [22] [23] [24] [20] [25] [26]. There was no obvious shift in the peak position of the chazabite framework of the SAPO-34 due to the single – metal substitution. The only noticeable shift in the diffraction pattern was due to the high gallium loading observed at 2theta = 22.5°.

It can also be observed that the crystallinity of the catalysts is consistent with no obvious amorphous phase with this metal loading.

The crystal sizes in Figure 4.2 are different for the various catalysts investigated which could be attributed to the difference in ionic radius, atoms, and the level of isomorphous substitution [27] [28]. According to Ione et al, the favorable outcome of isomorphous

substitution depends on the coordination number after substitution, ionization potentials of atoms involved in the substitution process, the ratio of the atoms participating in the process, electronegativity ratio, and charge difference of the atoms involved in the substitution. The ease of substitution occurs when $\Delta r/r \leq 0.15$, where r is the radius of the atom to be substituted in the framework. A sizeable atom can substitute little atom if the substitution generates a coordination number of the atom been replaced is low and contrariwise. The effect of ionic radius could be reflected in the crystallization of the atom been substituted, an increase in the ionic radius could lead to an increase in the activation energy thereby slowing down the crystallization of the atom with the material. The ionic radius of the different atom participating in the substitution increases in this order Al<Cr<Ga<V<In. The Al atom is considered the atom been substituted because of the high $\Delta r/r$ associated with P and Si substitution. Based on the findings of Kang and Lee [29], the ease of replacing the atom decrease in this order Cr>Ga>V>In. it should also be noted that there was no obvious diffraction peak from the XRD pattern associated with the single - metals substitution, suggesting the uniformity of the substituted metal and the support.

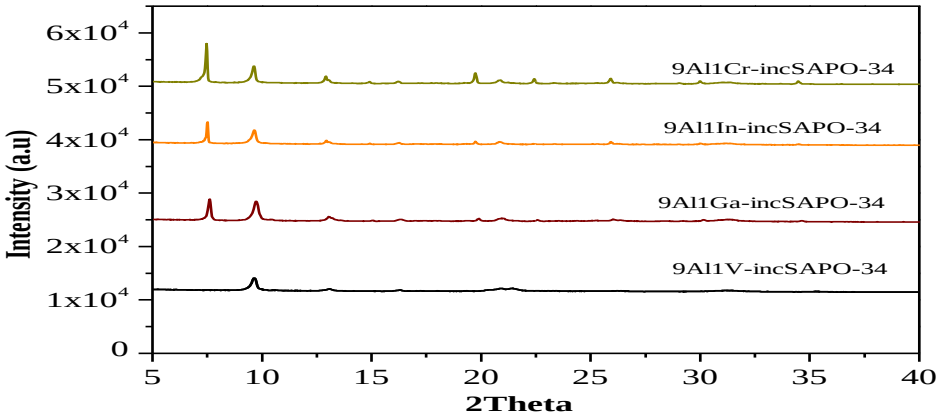

Figure 4.1. XRD Pattern of Catalysts Investigated

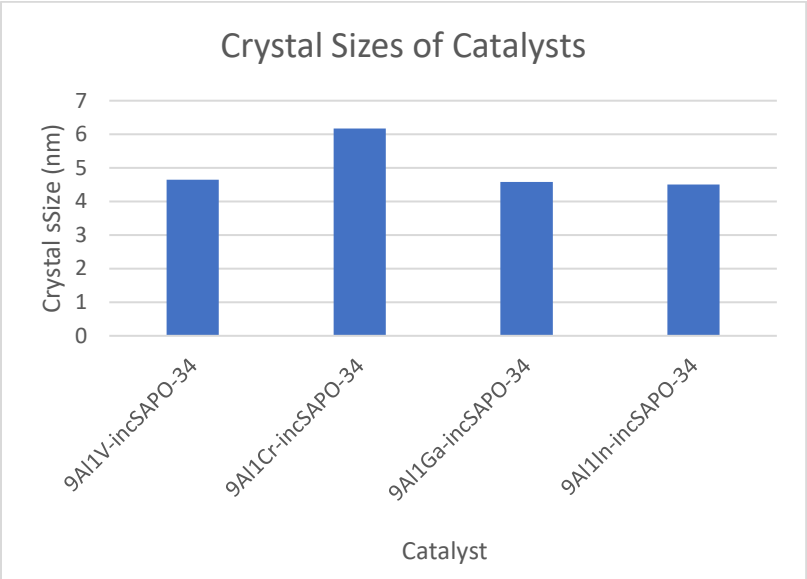

Figure 4.2. Crystal Sizes of the Prepared Catalysts

4.2. SCANNING ELECTRON MICROSCOPY (SEM) ANALYSIS OF CATALYST

The determination of the topology and the morphology is important to understand the hierarchical structure of these catalysts. The result of the SEM image of the catalysts is shown in Figure 4.3. The SAPO-34 has a rhombohedra morphology with 0.67 0.67µm mean size. It has a sheet-like structure while the triangular crystal could be a result of the crystallization of unreacted species. At low Ga loading, the particle retained a uniform structure with negligible distortion of the zeolite structure. An amorphous structure was observed with low In loading, high V, Ga, and In metal loading as shown in Figure 4.1 above. It can be observed from the XRD pattern that at high metal loading, there are stunted peak intensities, resulting in a decrease in crystallinity. The increase in metal (Ga)

loading don't necessarily affect the crystallinity of the zeolite but could be attributed to the nuclei forming the zeolite which is in agreement with literature [29] [30].

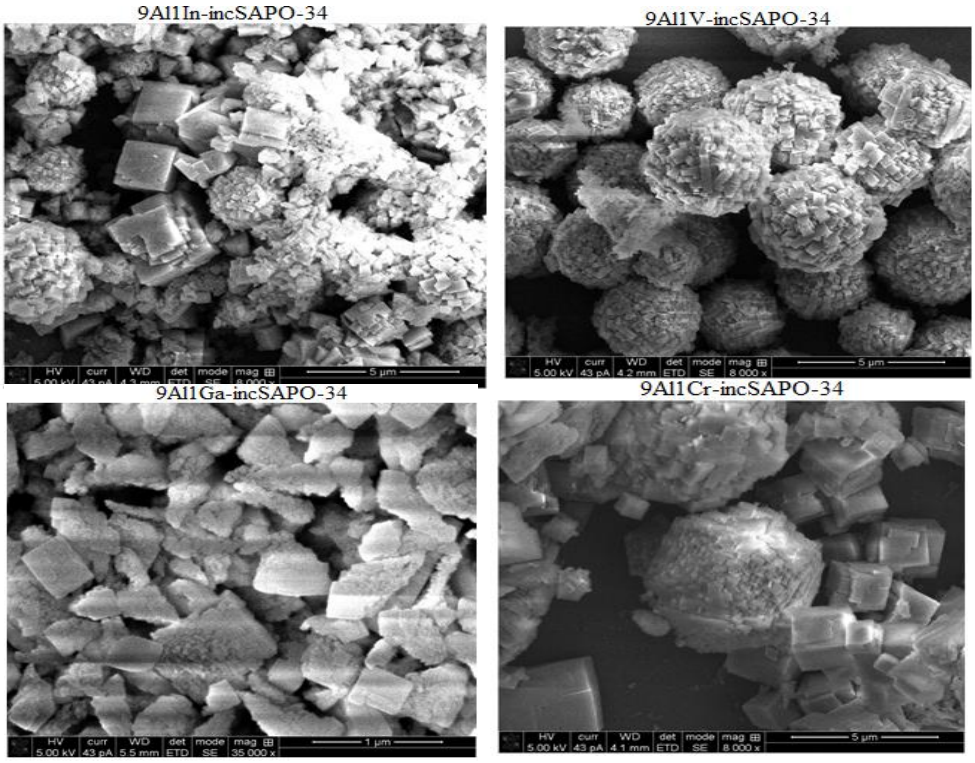

Figure 4.3. SEM Images for the Four Catalysts

4.3. NITROGEN PHYSISORPTION ANALYSIS

The textural properties, the pore volume, BET surface area, pore size, and analysis of the adsorption isotherm were carried out using the N_2 adsorption-desorption isotherm as shown in Figure 4.4 and Table 4.1 respectively. The isotherm for the four catalysts investigated shows a classic type 4 isotherm based on the IUPAC categorization [34]. At lower pressure, a moderately precipitous adsorption of the isotherm was observed suggesting the existence of microporous structure. At medium and high pressures, a type

H4 hysteresis curve is observed. This observation occurred at a comparatively high pressure say (P/P_0 of 0.8-1) for the zeolite support, and lower loading of Ga substituted catalyst. The hysteresis curve was also observed for the V, In, and Cr substituted catalyst at P/P_0 of 0.45 – 1. This also suggests the presence of a mesopore structure following the isomorphous substitution of the various metals, and this hysteresis curve/loop increases with an increase in metal loading. The presence of the observed mesopore is as a result of the formation of interspace originating from the close assembly of the crystalline particle, which is in agreement with literature [31]. Catalytic activity is also enhanced by the presence of mesoporous structure [31] [32].

This technique was also used to obtain the BET surface area of the calcined four catalysts investigated. At low metal loading, there was an increase in the specific surface area and pore volume, but there is also a decrease in the pore size of the V, and Cr substituted catalysts. The significant increase in the BET surface area could be attributed to the crystallization of tiny particles resulting from the solidification of nuclei at high metal loading.

The increase in the pore volume of the samples investigated could be a result of the collection of crystals particles as shown in Table 4.3. The pore volume of catalysts has a positive effect by affecting the structural position of catalysts, thereby mitigating mass transfer limitations and thus improving catalytic activity [33]. The importance of using the isomorphous method cannot be over-emphasized. This method was used because of its importance in increasing the specific surface area, pore volume, and the formation of mesopore structure. This was achieved by the dispersal of the metal species in the pores of the zeolite CHA framework in agreement with literature [30] [34]. This method,

isomorphous substitution was used against the conventional impregnation method, because the impregnating or doping the SAPO-34 zeolite support with metal, has the tendency of reducing the surface area and pore volume of the chazabite framework of the support which occurs when the metal is positioned on the surface and pore entrance of the zeolite support.

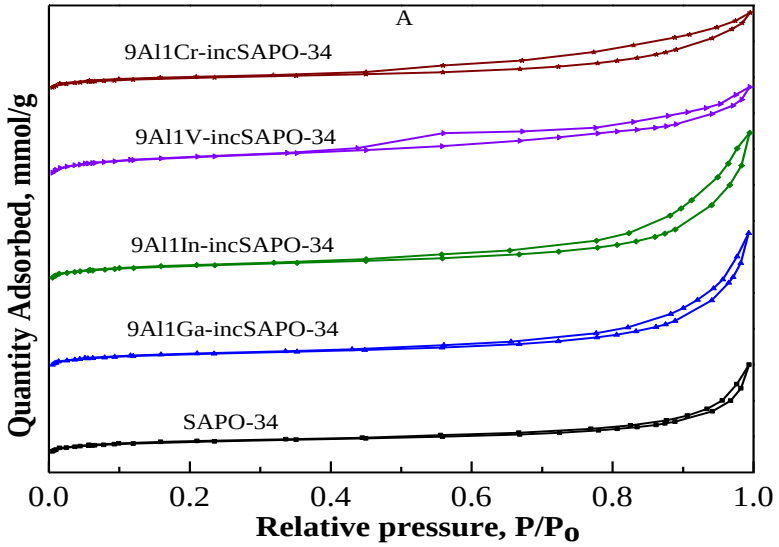

Figure 4.4. N_2 Adsorption-Desorption Isotherms for Different Catalysts Investigated

4.4. TEMPERATURE PROGRAMMED DESORPTION OF AMMONIA (NH_3 – TPD) ANALYSIS

The determination of acid-base properties of the catalyst is essential in understanding the metal supports interaction. The activation of the Methane molecules dominate in an acidic environment. This technique helps analyze the quantity of Bronsted and Lewis acid sites in catalysts [19]. Figure 4.6 represents the acid sites measured from an NH_3-TPD profile of substituted metals. The acid sites are measured from the NH_3-TPD profile, utilizing the integration tool. The observation of two distant peaks from the NH_3-

TPD profile is shown in Figure 4.5 below suggests the presence of weak acid sites between 100 and 250˚C on the Si-O-Si and strong acid sites associated with the Al species framework [35] [36].

Table 4.1. Textural Properties of the Different Catalysts

Catalyst	$S_{BET,}$ (m^2/g)	Pore size (nm)	*Micropore* $vol.\,cm^3/g$	*Mesopore* $vol.\,cm^3/g$	*Totalpore* $vol.\,cm^3/g$
SAPO-34	456	14.00	0.08	0.18	0.26
9Al1V-incSAPO-34	647	9.58	0.09	0.25	0.34
9Al1Cr-incSAPO-34	584	11.82	0.06	0.24	0.31
9Al1Ga-incSAPO-34	610	20.39	0.13	0.24	0.37
9Al1In-incSAPO-34	564	19.93	0.14	0.22	0.36

The interactivity between the reacting molecule (CH_4 and CO_2) and the catalyst, as well as the interplay between the catalyst and NH_3, can be found quantitatively using the desorption temperature [37]. A strong interplay between the acid and NH_3 (probe molecule) is achieved when the NH_3 is desorbed at a higher energy as a result of a high desorption temperature.

Based on the NH_3-TPD profile, the metal substituted catalysts have a lower Bronsted and Lewis acidic properties compared to the SAPO-34 zeolite support. Increasing the metal loading (lower Al metal ratio) could decrease the Bronsted and Lewis acid sites. The implications of this is the isomorphous substitution of Al is achieved. The

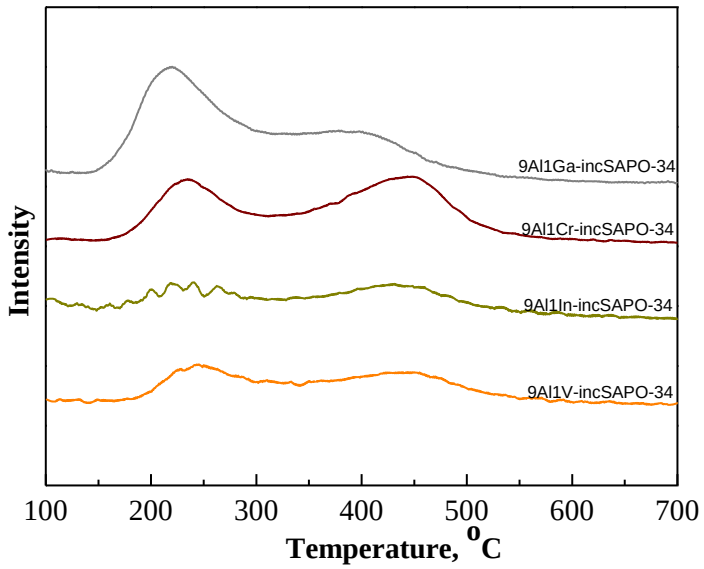

Figure 4.5. NH_3-TPD Profile of the Catalysts

addition of different metals have different effects on the acidity of the catalyst. The surface acidity of the catalyst is increased by the incorporation of Ga, which contradicts the isomorphous substitution of Ga in SAPO-34 [38].

The addition of Ga leads to an increase in Bronsted acidity; the low loading of V increased the Lewis acidity (surface acidity). High catalytic activity can be achieved for the Ga substituted metal due to its strong metal-support interaction based on its strong Bronsted acid sites, which is an agreement with those reported in literature by Xu et. al., but it contradicts the observation Zhang et. al. [39] [30] [34].

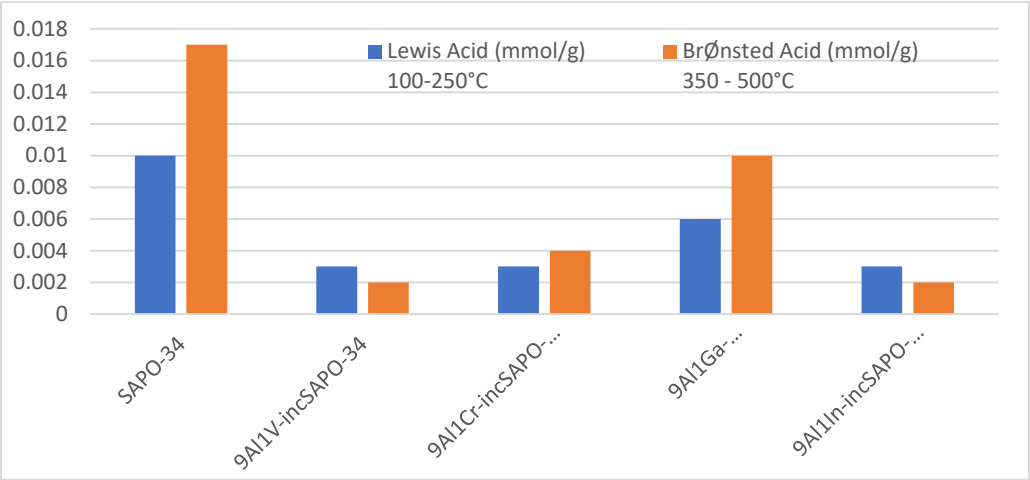

Figure 4.6. Measured BrØnsted and Lewis Acidity of Catalysts

4.5. CATALYTIC ACTIVITY

The data obtained from the online gas chromatograph was analyzed for CH_4 and CO_2 conversion, H_2 and CO selectivity, as well as the overall catalytic activity, was determined for the four catalysts that were tested during the 6.5h on stream. The catalysts resulted in different conversion of CH_4, while the Cr promoted catalyst showed a linear CH_4 conversion with time as shown in Figure 4.7. The CO_2 conversion showed a linear conversion for 9Al 1V-inc SAPO-34, 9Al1Ga-inc SAPO-34, and 9Al 1Cr-inc SAPO-34 for the 6.5h. on-stream, while 9Al 1In-inc SAPO-34 showed a little deviation at 4h. on-stream and had a constant conversion for the remaining time on stream. The activity of the catalysts for CO_2 conversion as shown in Figure 4.8 could be attributed to different geometry and electron transfer interactions of the alloys. The stability of CO_2 conversion could stem from the thermally stable, well-defined microporous structure (Chabazite framework) support used, which also have a high affinity for CO_2. This is in agreement

with that reported in literature [15]. The catalysts tested gave different conversions at various times on stream. The highest conversion for CH_4 was obtained as follows: 9Al 1V-inc SAPO-34 (27%), 9Al 1Cr-inc SAPO-34 (33%), 9Al 1Ga-inc SAPO-34 (31%), and 9Al 1In-inc SAPO-34 (32%).

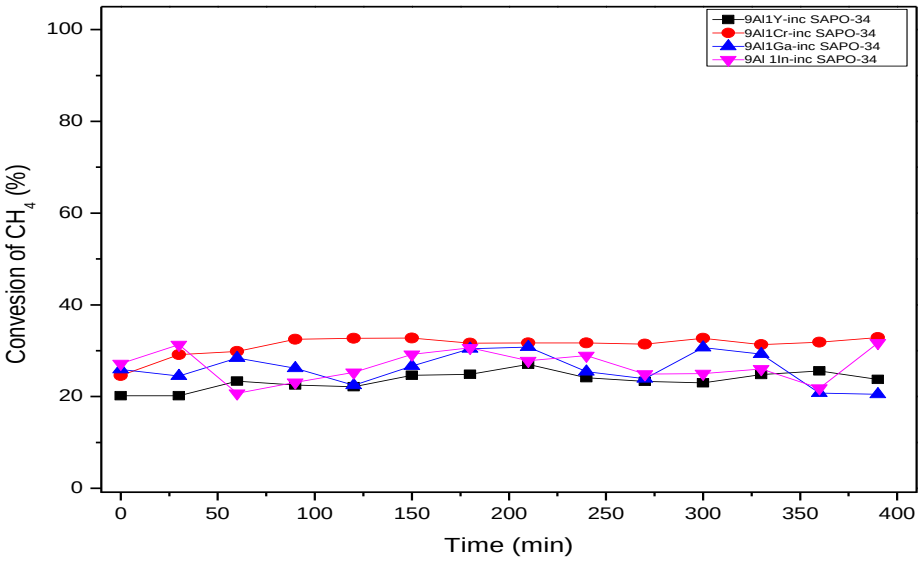

Figure 4.7. Conversion of CH_4 for Different Catalysts

The Cr promoted catalyst gave the highest conversion due to the attribution of the six valence electrons, and/or geometry, which has the ability to decrease the aluminum ensemble creating a well-dispersed phase/active site for the activation of the CH_4 molecule suggesting that 9Al 1Cr-inc SAPO-34 is the active catalyst for the dry reforming of methane. The high conversion of the Cr promoted catalyst could also be attributed to the ease of substitution of the Cr atom.

The different conversions obtained for CH_4 could be due to the difference in the dispersion because of the interaction of the alloys, the difference in geometry, and/or

electron densities. The different conversions obtained for CH_4 could be due to the difference in the dispersion because of the interaction of the alloys, the difference in geometry, and/or electron densities.

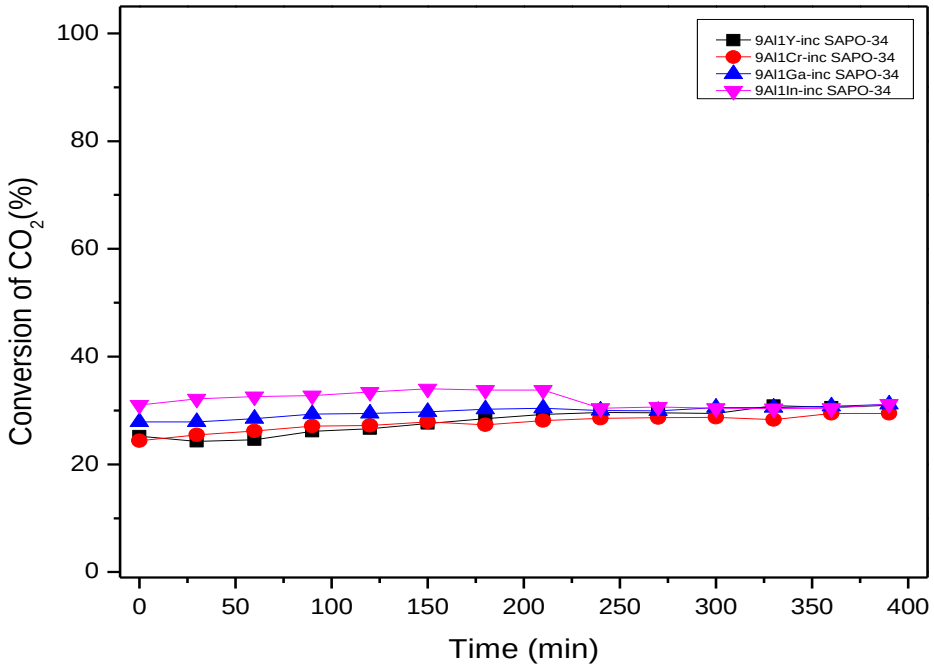

Figure 4.8. Conversion of Carbon Monoxide (CO_2)

In Figure 4.8 , the four catalysts tested also showed a consistent conversion for CO_2. The carbon dioxide activates on the SAPO-34 Bronsted acid support, which has a strong affinity for CO_2. Similarly, the highest conversion of CO_2 for the different catalysts are as follows: 9Al 1V- inc SAPO-34 (30.96%), 9Al 1Cr- inc SAPO-34 (29.42%), 9Al-1Ga inc SAPO-34 (32.7%), and 9Al-1In -inc SAPO-34 (33.79%).

The In promoted catalyst is not active towards DRM as shown in Table 4.1 because it was not selective towards H_2. This could be due to the dehydrogenation and RWGS

reaction pathway [Eq. (4)] as reported in literature, but the In promoted catalyst gave the highest CO_2 conversion, which could be due to its strong metal-support interaction (SMSI). The catalysts tested did not show a significant deactivation during the 6.5h on-stream because of the stability of the zeolite catalyst, which is in agreement with that reported in literature [15]. The stability of the catalyst could also be due to the different promoters used as they could also be responsible for the oxidation of the accumulated coke formed on the Al sites [40]. The different selectivity of these catalysts could be attributed to the different promoters incorporated via the isomorphous substitution. The Vanadium (V) promoted catalyst gave the highest selectivity of H_2 and CO_2 as shown in Table 4.2 due to its large surface area, needed for the reaction to take place, calculated from the BET experiment.

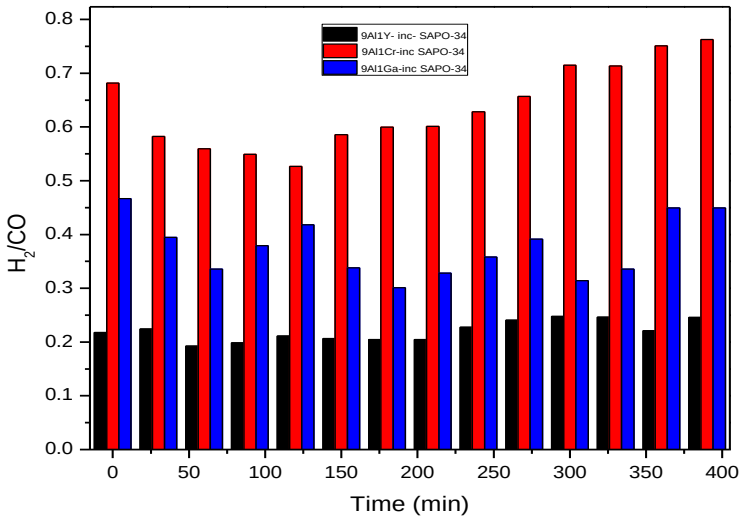

Figure 4.9. Syngas Ratios for Different Catalysts

The syngas ratios for the four catalysts were also computed, and it was observed that the catalyst 9Al-1Cr inc SAPO-34 had the highest syngas ratio as shown in Figure 4.9

and Table 4.2. The Ga substituted metal or promote d catalyst has the same conversion for CH_4 and CO_2 which could be due to its strong metal-support interactions. Based on analysis, the Cr promoted catalyst could be the best choice for the F-T process due to the fact it gave a syngas ratio of 0.76 to its high CH_4 conversion, which is in strong agreement with that reported thermodynamically in literature [40].

Table 4.2. Catalytic Performance of Different Catalysts

Catalyst	X_{CH_4} (%)	X_{CO_2} (%)	S_{H_2} (%)	S_{CO} (%)	H_2/CO
9Al1V-incSAPO-34	27	31	7	34	0.2
9Al1Cr-incSAPO-34	33	29	6	9	0.7
9Al1Ga-incSAPO-34	31	31	6	14	0.5
9Al1In – incSAPO-34	32	34	-	6	-

It became necessary to also investigate the effect of mass and heat transfer limitations on these catalysts to ascertain their prospects for commercialization. Based on the Weiz – Prater criterion for internal diffusion from Table 4.3, there are no diffusion limitations and, as a result, no concentration gradient within the pellet of the three catalysts investigated. Since the effect of external diffusion was evaluated by Mears criterion, there is no concentration gradient between the bulk gas phase and the surface of the catalysts.

Based on the investigation using the Mears Criterion to investigate the effect of external heat transfer on the three catalysts, it can be inferred that there are no heat transfer

limitations as shown in Table 4.3. Based on the analysis carried out using these criteria, no limitation exists on heat and mass transfer within the catalyst as shown in Table 4.3.

Table 4.3. Mass and Heat Transfer Limitations for Different Catalysts

Catalyst	$-r_A(kmol/kg_{cat}\bullet s)$	C_{WP} (Int.Diff.)	Mears Criteria (Ext. Diff.)	Mears Criteria (Ext.Heat Tran.)	CIIHMT
9Al1V-incSAPO-34	$2.61*10^{-4}$	$5.8*10^{-5}<1$	$8.2*10^{-8}<0.15$	$0.13<0.15$	$5.2*10^{-8}<1$
9Al1Cr-incSAPO-34	$2.01*10^{-4}$	$5.1*10^{-6}<1$	$3.8*10^{-9}<0.15$	$0.08<0.15$	$4.1*10^{-9}<1$
9Al1Ga-incSAPO-34	$2.37*10^{-4}$	$1.8*10^{-6}<1$	$6.1*10^{-9}<0.15$	$0.12<0.15$	$1.2*10^{-9}<1$

5. CONCLUSIONS

The performance of the four catalysts gave different conversion, selectivity, and syngas ratio. This observation is because of the different promoters which influenced the metal-support interaction, even though they have the same support. The degree of the isomorphous substitution of the different metal also played a vital role that influenced the observed conversion for CH_4 and CO_2. The promoters also influence the dispersion of the active sites for the activation of the methane molecule, which is in agreement with the different conversions observed for the different catalysts. The Chromium promoted catalyst gave the highest syngas ratio of 0.7, which can be further utilized for the Fischer-Tropsch process in producing liquid fuels and other hydrocarbons. The DRM for commercial purposes is still an ongoing research area, and we believe that this research work can be improved by further doping or promoting these catalysts especially the 9Al 1Cr – inc SAPO-34 with suitable metals. The commercialization of these catalysts could also be possible because there are no heat and mass transfer limitations. Based on these findings and from previous research work, the DRM process is still a very attractive research topic in establishing the best process for its commercialization.

REFERENCES

[1] M.S. Fan, A.Z. Abdullah, S. Bhatia, Catalytic technology for carbon dioxide reforming of methane to synthesis gas, ChemCatChem. 1 (2009) 192–208. https://doi.org/10.1002/cctc.200900025.

[2] K. Narsimhan, K. Iyoki, K. Dinh, Y. Román-Leshkov, Catalytic oxidation of methane into methanol over copper-exchanged zeolites with oxygen at low temperature, ACS Cent. Sci. 2 (2016) 424–429. https://doi.org/10.1021/acscentsci.6b00139.

[3] C. Egawa, Methane dry reforming reaction on Ru(0 0 1) surfaces, J. Catal. 358 (2018) 35–42. https://doi.org/10.1016/j.jcat.2017.11.010.

[4] P. Cao, S. Adegbite, H. Zhao, E. Lester, T. Wu, Tuning dry reforming of methane for F-T syntheses: A thermodynamic approach, Appl. Energy. 227 (2018) 190–197. https://doi.org/10.1016/j.apenergy.2017.08.007.

[5] T. Stroud, T.J. Smith, E. Le Saché, J.L. Santos, M.A. Centeno, H. Arellano-Garcia, J.A. Odriozola, T.R. Reina, Chemical CO 2 recycling via dry and bi reforming of methane using Ni-Sn/Al 2 O 3 and Ni-Sn/CeO 2 -Al 2 O 3 catalysts, Appl. Catal. B Environ. 224 (2018) 125–135. https://doi.org/10.1016/j.apcatb.2017.10.047.

[6] S.M. Nicholson, D. Goms, B. De Nchaud, R. Bruzzone, Altered gene expression in Schwann cells of connexin32 knockout animals, J. Neurosci. Res. 66 (2001) 23–36. https://doi.org/10.1016/j.cattod.2013.05.023.

[7] U. Guharoy, E. Le Saché, Q. Cai, T.R. Reina, S. Gu, Understanding the role of Ni-Sn interaction to design highly effective CO 2 conversion catalysts for dry reforming of methane, J. CO2 Util. 27 (2018) 1–10. https://doi.org/10.1016/j.jcou.2018.06.024.

[8] M. Yu, K. Zhu, Z. Liu, H. Xiao, W. Deng, X. Zhou, Carbon dioxide reforming of methane over promoted NixMg1-xO (111) platelet catalyst derived from solvothermal synthesis, Appl. Catal. B Environ. 148–149 (2014) 177–190. https://doi.org/10.1016/j.apcatb.2013.10.046.

[9] D. Pakhare, J. Spivey, A review of dry (CO2) reforming of methane over noble metal catalysts, Chem. Soc. Rev. 43 (2014) 7813–7837. https://doi.org/10.1039/c3cs60395d.

[10] Z. Nawaz, X. Tang, Q. Zhang, D. Wang, W. Fei, SAPO-34 supported Pt-Sn-based novel catalyst for propane dehydrogenation to propylene, Catal. Commun. 10 (2009) 1925–1930. https://doi.org/10.1016/j.catcom.2009.07.008.

[11] Y. Li, Y. Huang, J. Guo, M. Zhang, D. Wang, F. Wei, Y. Wang, Hierarchical SAPO-34/18 zeolite with low acid site density for converting methanol to olefins, Catal. Today. 233 (2014) 2–7. https://doi.org/10.1016/j.cattod.2014.03.038.

[12] L. Ye, F. Cao, W. Ying, D. Fang, Q. Sun, Effect of Different TEAOH/DEA Combinations on SAPO-34's Synthesis and Catalytic Performance, J. Porous Mater. 18 (2011) 225–232.

[13] E. Dumitriu, A. Azzouz, V. Hulea, D. Lutic, H. Kessler, Synthesis, characterization and catalytic activity of SAPO-34 obtained with piperidine as templating agent, Microporous Mater. 10 (1997) 1–12.

[14] G. Sastre, D.W. Lewis, C. Richard, A. Catlow, Modeling of silicon substitution in SAPO-5 and SAPO-34 molecular sieves, J. Phys. Chem. B. 101 (1997) 5249–5262. https://doi.org/10.1021/jp963736k.

[15] A.H. Fakeeha, W.U. Khan, A.S. Al-Fatesh, A.E. Abasaeed, Stabilities of zeolite-supported Ni catalysts for dry reforming of methane, Cuihua Xuebao/Chinese J. Catal. 34 (2013) 764–768. https://doi.org/10.1016/S1872-2067(12)60554-3.

[16] J.J. Spivey, G. Hutchings, Catalytic aromatization of methane, Chem. Soc. Rev. 43 (2014) 792–803. https://doi.org/10.1039/c3cs60259a.

[17] S.A. Theofanidis, V. V. Galvita, H. Poelman, G.B. Marin, Enhanced carbon-resistant dry reforming Fe-Ni catalyst: Role of Fe, ACS Catal. 5 (2015) 3028–3039. https://doi.org/10.1021/acscatal.5b00357.

[18] S.T. Oyama, X. Zhang, J. Lu, Y. Gu, T. Fujitani, Epoxidation of propylene with H 2 and O 2 in the explosive regime in a packed-bed catalytic membrane reactor, J. Catal. 257 (2008) 1–4. https://doi.org/10.1016/j.jcat.2008.04.023.

[19] J.G. Post, J.H.C. van Hooff, Acidity and activity of H-ZSM-5 measured with NH3-t.p.d. and n-hexane cracking, Zeolites. 4 (1984) 9–14. https://doi.org/10.1016/0144-2449(84)90065-4.

[20] S.R. Venna, M.A. Carreon, Synthesis of SAPO-34 crystals in the presence of crystal growth inhibitors, J. Phys. Chem. B. 112 (2008) 16261–16265. https://doi.org/10.1021/jp809316s.

[21] B. Vistad, D.E. Akporiaye, K.P. Lillerud, Identification of a key precursor phase for synthesis of SAPO-34 and kinetics of formation investigated by in situ X-ray diffraction, J. Phys. Chem. B. 105 (2001) 12437–12447. https://doi.org/10.1021/jp0110758.

[22] Z. Nawaz, F. Wei, Hydrothermal study of Pt-Sn-based SAPO-34 supported novel catalyst used for selective propane dehydrogenation to propylene, J. Ind. Eng. Chem. 16 (2010) 774–784. https://doi.org/10.1016/j.jiec.2010.07.002.

[23] Y. Cheng, H. Gong, C. Miao, W. Hua, Y. Yue, Z. Gao, Ga<inf>2</inf>O<inf>3</inf>/HSSZ-13 for dehydrogenation of ethane: Effect of pore geometry of support, Catal. Commun. 71 (2015) 42–45. https://doi.org/10.1016/j.catcom.2015.08.015.

[24] A. Izadbakhsh, F. Farhadi, F. Khorasheh, S. Sahebdelfar, M. Asadi, Y.Z. Feng, Effect of SAPO-34's composition on its physico-chemical properties and deactivation in MTO process, Appl. Catal. A Gen. 364 (2009) 48–56. https://doi.org/10.1016/j.apcata.2009.05.022.

[25] M.M.. Treacy, J.B. Higgins, Collection of Simulated XRD Powder Patterns for Zeolites Fifth (5th) Revised Edition, 2007.

[26] J. Gong, C. Wang, C. Zeng, L. Zhang, Hydrothermal preparation of hierarchical SAPO-34 constructed by nano-sheets using rapeseed pollen extract as water and its CO2 adsorption property, Microporous Mesoporous Mater. 221 (2016) 128–136. https://doi.org/10.1016/j.micromeso.2015.09.035.

[27] R. Fricke, H. Kosslick, G. Lischke, M. Richter, Incorporation of gallium into zeolites: syntheses, properties and catalytic application, Chem. Rev. 100 (2000) 2303–2405. https://doi.org/10.1021/cr9411637.

[28] K.G. Ione, L.A. Vostrikova, The Isomorphism and Catalytic Properties of Silicates with the Zeolite Structure, Russ. Chem. Rev. 56 (1987) 231–251.

[29] M. Kang, C.-T. Lee, Synthesis of Ga-incorporated SAPO-34s (GaAPSO-34) and their catalytic performance on methanol conversion, J. Mol. Catal. A Chem. 150 (1999) 213–222.

[30] Y. Zhang, Y. Zhou, L. Huang, S. Zhou, X. Sheng, Q. Wang, C. Zhang, Structure and catalytic properties of the Zn-modified ZSM-5 supported platinum catalyst for propane dehydrogenation, Chem. Eng. J. 270 (2015) 352–361. https://doi.org/10.1016/j.cej.2015.01.008.

[31] H. Yang, Z. Liu, H. Gao, Z. Xie, Synthesis and catalytic performances of hierarchical SAPO-34 monolith, J. Mater. Chem. 20 (2010) 3227–3231. https://doi.org/10.1039/b924736j.

[32] N. Linares, A.M. Silvestre-Albero, E. Serrano, J. Silvestre-Albero, J. García-Martínez, Mesoporous materials for clean energy technologies, Chem. Soc. Rev. 43 (2014) 7681–7717. https://doi.org/10.1039/c3cs60435g.

[33] B.O. Dalla Costa, M.A. Peralta, C.A. Querini, Gas phase dehydration of glycerol over, lanthanum-modified beta-zeolite, Appl. Catal. A Gen. 472 (2014) 53–63. https://doi.org/10.1016/j.apcata.2013.12.011.

[34] Y. Zhang, Y. Zhou, L. Huang, M. Xue, S. Zhang, Sn-modified ZSM-5 As support for platinum catalyst in propane dehydrogenation, Ind. Eng. Chem. Res. 50 (2011) 7896–7902. https://doi.org/10.1021/ie1024694.

[35] Y. Zhang, Y. Zhou, A. Qiu, Y. Wang, Y. Xu, P. Wu, Effect of Na Addition on Catalytic Performance of PtSn/ZSM-5 Catalyst for Propane Dehydrogenation, Acta Physico-Chimica Sin. 22 (2006) 672–678.

[36] S. Zhou, Y. Zhou, Y. Zhang, X. Sheng, Z. Zhang, J. Kong, Synthesis of core-shell-structured SBA-15@MgAl2O4 with enhanced catalytic performance of propane dehydrogenation, J. Mater. Sci. 49 (2014) 1170–1178. https://doi.org/10.1007/s10853-013-7797-4.

[37] S. Blanco, S.R.G. Carrazán, V. Rives, Oxidative dehydrogenation of propane on Mg-V-Al mixed oxides, Appl. Catal. A Gen. 342 (2008) 93–98. https://doi.org/10.1016/j.apcata.2008.03.002.

[38] M. Chen, J. Xu, F.Z. Su, Y.M. Liu, Y. Cao, H.Y. He, K.N. Fan, Dehydrogenation of propane over spinel-type gallia-alumina solid solution catalysts, J. Catal. 256 (2008) 293–300. https://doi.org/10.1016/j.jcat.2008.03.021.

[39] B. Xu, T. Li, B. Zheng, W. Hua, Y. Yue, Z. Gao, Enhanced stability of HZSM-5 supported Ga2O3 catalyst in propane dehydrogenation by dealumination, Catal. Letters. 119 (2007) 283–288. https://doi.org/10.1007/s10562-007-9232-4.

[40] B. Sarkar, R. Goyal, C. Pendem, T. Sasaki, R. Bal, Highly nanodispersed Gd-doped Ni/ZSM-5 catalyst for enhanced carbon-resistant dry reforming of methane, J. Mol. Catal. A Chem. 424 (2016) 17–26. https://doi.org/10.1016/j.molcata.2016.08.006.

VITA

Ojo Ehigiator Festus was born in Benin City, Nigeria. In November 2008, he graduated with a Bachelor in Engineering in Chemical Engineering from the University of Benin, Nigeria, in which he was awarded for second class (Upper Division). He joined the United States Air force in September 2016 and also worked for Amazon from September 2016 to December 2017.

He joined Missouri S&T in January 2018 and completed the requirements for graduate school. He obtained a Master of Science in Chemical Engineering from Missouri S&T in December 2019.